On the identification of Sb_2Se_3 using Raman scattering

A. Shongalova[1,2], M. R. Correia[1], B. Vermang[3,4,5], J. M.V. Cunha[6], P. M.P. Salomé[6,7] and P. A. Fernandes[1,6,8, #]

(1) Departamento de Física and I3N, Universidade de Aveiro, 3810-193 Aveiro, Portugal

(2) Satpayev University, Satpayev street, 22a, 050013 Almaty City, Kazakhstan

(3) University of Hasselt – partner in Solliance, Agoralaan gebouw H, Diepenbeek, 3590, Belgium

(4) Imec – partner in Solliance, Kapeldreef 75, Leuven, 3001, Belgium

(5) Imomec – partner in Solliance, Wetenschapspark 1, Diepenbeek, 3590, Belgium

(6) International Iberian Nanotechnology Laboratory, 4715-330 Braga, Portugal

(7) Departamento de Física, Universidade de Aveiro, 3810-193 Aveiro, Portugal

(8) CIETI, Departamento de Física, Instituto Superior de Engenharia do Porto, Instituto Politécnico do Porto, Rua Dr. António Bernardino de Almeida, 431, 4200-072 Porto, Portugal

corresponding author: P.A. Fernandes – paulo.fernandes@inl.int

Keywords: Antimony bi-selenide Sb_2Se_3, thin films, Raman scattering (RS), semiconductors

Abstract*:* Robust evidences are presented showing that the Raman mode around 250 cm^{-1} in the Sb_2Se_3 thin films does not belong to this binary compound. The laser power density dependence of the Raman spectrum revealed the formation of Sb_2O_3 for high values of laser intensity power density excitation under normal atmospheric conditions. To complement this study, the Sb_2Se_3 films were characterized by X-ray diffraction during in-situ annealing. Both these measurements showed that the Sb_2Se_3 compound can be replaced by Sb_2O_3. A heat-assisted chemical process explains these findings. Furthermore, Raman conditions required to perform precise measurements are described.

Introduction

Recent studies on semiconductor compound Sb_2Se_3 have shown that this material has many interesting properties for several applications: thermoelectric[1], energy storage devices[2–4], solar cells[1,5–9], among others. Sb_2Se_3 can be prepared in polycrystalline thin films with the orthorhombic crystalline structure using standard (both atmospheric pressure or vacuum based) thin film growth techniques like electrodeposition[10] or thermal evaporation[5,11], just to name a few. Sb_2Se_3 appears to be in the same class of materials as the chalcogenides $Cu(In,Ga)Se_2$ (CIGS), CdTe, $Cu_2ZnSn(S,Se)_4$ (CZTSSe), i.e. they have excellent optoelectronic properties and are self-doped semiconductors. Their doping is intrinsic to their crystalline structure and depends heavily on growth parameters and properties. Hence, the correct identification of the Sb_2Se_3 crystalline structure and the correct use of the corresponding identification techniques, are of the utmost importance for the advancement of this material as an application for optoelectronic devices.

The researchers have turned their attention to Raman scattering (RS) as a powerful technique to provide qualitative information about the crystal phase of chalcogenides materials [12,13]. RS is widely used for the identification of main and secondary phases of chalcogenide materials as it is a non-destructive technique and allows for very fast interpretations. Moreover, in the chalcogenide materials, RS usually allows for the identification of the dominant phases without superimposition problems, as it can occur in x-ray diffraction[14]. With regards to Sb_2Se_3, in the literature, the peaks at 190 cm^{-1} and 250 cm^{-1} are usually attributed to Sb-Se and Sb-Sb bonds, respectively[11,15,16]. However, the peak around 250 cm^{-1} has many interpretations and conflicting origins[15,17,18]. In fact, part of the assignment's problem arises from the fact of several selenium phases and antimony oxides having peaks close to that region as shown in Table 1. As the correct identification of which phases and structures will allow for a better understanding of the Sb_2Se_3 growth mechanisms and properties, in this work we will show that: i) the 250 cm^{-1} peak does not belong

to the Sb_2Se_3 phase and ii) RS measurements done at high laser power density conditions lead to oxidation of the sample surface.

Experimental procedure

The Sb_2Se_3 thin films were grown according to a two-step process. Se-rich Sb-Se thin films were sputtered from a Sb_2Se_3 sputtering target (Stanford Advanced Materials) with a 99.99% purity, followed by a rapid thermal annealing at 300 ^oC with H_2Se during 15 minutes. Composition was analyzed using Energy Dispersive Spectroscopy and the composition ratio, [Se]/[Sb], is 1.9, which by comparing with the stoichiometric value of 1.5, implies that the overall sample is Se rich. Such fact is normal in this kind of samples as widely reported, due to condensation of Se during the cooling down of the film. Optical reflectance measurements allowed estimating a direct band gap energy of ~ 1.0 eV. The RS measurements were done in the backscattering configuration using a Jobin-Yvon LabRaman HR 800 spectrometer equipped with a multichannel air cooled (-70°C) CCD detector, an Olympus BX41 microscope. The surface of the sample was focused with the help of a long working distance (25 mm) 50 X objective having a numerical aperture of 0.45, allowing for a laser spot diameter of ~1.7 μm when a HeNe laser line (632.8 nm) is used as excitation source. The crystalline phase identification was complemented with X-ray diffraction measurements and the results indicate that orthorhombic *Pbnm* (62) Sb_2Se_3 is the dominant phase.

Results and discussion

In FIG. 1a) we present the Raman spectra of a Sb_2Se_3 film, measured for different power densities of the incident laser line, ranging from 170 MW/m^2 to 2180 MW/m^2, and under the same conditions of integration time and number of repetitions. In order to eliminate the influence of exposure time to laser incidence during the acquisition of each Raman spectrum, a previous study (not shown) of the temporal evolution of the Raman spectrum under continuous laser incidence was carried out for each of the laser power densities used. This allowed determining the maximum exposure time (50 s) for each laser power

density without changing the spectral shape. Moreover, for all our studies, the laser was turned off between each acquisition. The total laser incidence time required to perform all the spectra shown in FIG. 1a) was about 4 minutes. The Raman spectra show a pronounced dependence on the laser excitation power density. We note that similar studies carried out on orthorhombic Bi_2S_3 nanostructures[19] also have shown a strong dependence on power density excitation. In our case, all of the Raman spectra display peaks at 153 cm^{-1}, 189 cm^{-1} and 210 cm^{-1} commonly assigned to the Sb_2Se_3 phase. Under low power densities conditions there is a double peak at 234 cm^{-1} and 238 cm^{-1} which we attribute to trigonal Se[17], the most stable phase of Selenium[20]. The presence of such peak is consistent with the EDS measurements that showed a slight Se-rich film composition, and consequently, Se can condensate at the sample´s surface[21,22], which is very common in the preparation of this kind of samples. Intriguing is the evolution of the spectrum with increasing excitation power density. It should be noted that for the lowest laser power density, no peak at ~ 250 cm^{-1} is observed, in spite of this being one of the peaks commonly reported in the Raman studies of Sb_2Se_3[11,15,16,23]. As the laser power density increases, together with the appearance of the ~ 250 cm^{-1}peak other peaks (~ 80 cm^{-1}, ~ 372 cm^{-1}, and ~ 450 cm^{-1}) are detected whose intensities follow the increase on the intensity of the ~ 250 cm^{-1} peak, suggesting that they are likely connected. Furthermore, FIG. 1a) shows a clear decrease of the double peak located at ~ 235 cm^{-1} with increasing RS laser power until it vanishes, for the highest power density value. On the other hand, the peak located at 190 cm^{-1} remains, within the experimental error, stable in position and integrated intensity but its FWHM decreases by about 2 cm^{-1}. The well-known laser heating effect always causes anharmonic effects in solids, evidenced by a broadening and a red shift of the Raman bands[24], and simultaneously, under high power or prolonged laser irradiation, structural transitions and crystalline changes may occur due to long-range ordering, as well as local or macroscopic ordering[25]. At first glance one might think that the decrease of the FWHM of the peak at 190 cm^{-1} is related to the local annealing of the Sb_2Se_3 phase, which results in an improvement in the crystalline quality of the material. However, if this would be the case, one would

expect a gradual increase in intensity throughout the experiment, which was not observed. Consequently, it is unlikely that the peaks at 190 cm^{-1} and 250 cm^{-1} could be correlated, thus, we do not attribute the 250 cm^{-1} peak to the Sb_2Se_3 orthorhombic phase. The appearance of the 250 cm^{-1} peak will be discussed further in the text.

By comparing the values at ~ 80 cm^{-1}, ~189 cm^{-1}, ~ 372 cm^{-1} and ~ 250 cm^{-1} and ~ 450 cm^{-1} for the several phases summarized in Table 1, we concluded that these peaks correspond to a Sb_2O_3 phase. Previous Raman studies do not mention the power density used, and such experiments are commonly performed in air atmosphere. Those evidences lead us to affirm that the commonly reported Raman spectra are measured under high laser power density conditions, since the presence of the Raman peak at ~250 cm^{-1} is only observed in our measurements with high excitation power density conditions. In addition, due to the excess of Se in the films, Se phases are also a candidate to explain the existence of a Raman band at ~250 cm^{-1}, that is related with the vibration mode of Se_8 and Se_6 rings[17]. Taking into account the EDS results, showing an inhomogeneous Se distribution, different points of the sample were probed by Raman. With the objective of analyzing a region of the sample without a prolonged exposure to air, the sample was cut perpendicularly to the surface, and the Raman spectrum was immediately recorded at the fresh cross-section. FIG. 1b) relates the Raman spectrum measured, in air, close to the glass substrate, i.e. as further away from the surface of the film as possible. We do not expect Se condensation and oxidization of a fresh cleavage cross-section. Although the signal-to-noise ratio worsens, no peak at 250 cm^{-1} is observed by increasing the laser power density, and the observed main peaks can only be assigned to the Sb_2Se_3 phase. These results indicate that in this region the film has a well-defined stoichiometry, avoiding the probability of oxidation of Sb or the contribution of selenium condensates.

All the Raman peaks observed in FIG. 1a) and FIG. 1b) are within the expected range of frequencies when compared with the Raman frequencies reported for the lighter Sb_2S_3 isostructural phase[26]. The

group theory predicted, for the Sb_2Se_3 unit cell of five non-equivalent sites, thirty zone-center Raman actives phonon modes belonging to the irreducible representation: $\Gamma_{Raman} = 10\,A_g + 10\,B_{1g} + 5\,B_{2g} + 5\,B_{3g}$. Removing the zero-frequency acoustic phonon modes, a total of twenty seven optical Raman modes are expected[26,27]. In spite of the huge number of phonons expected, only few peaks have been observed in the Raman studies reported so far[15,16,28–30]. In the Raman study reported by Y. Zhao et al[19] for high quality samples of Bi_2S_3 material, which is also isostructural to Sb_2Se_3, the number of experimental Raman peaks observed is higher than the commonly observed ones for Sb_2Se_3. In that work, the comparison between theoretical and experimental frequencies was possible considering an adjustment process involving the entire Raman spectrum, neglecting other contributions. We note that if Sb_2Se_3 and Bi_2S_3 are isostructural with the orthorhombic crystalline phase, then, one would expect the peaks of both phases to be visible close in energy positions and with the same number of modes. Such fact is true if we discard the 250 cm^{-1} peak. Such occurrence is another indication supporting the hypothesis that this peak is not from the Sb_2Se_3 phase. As the crystalline structure of Sb_2O_3 is cubic, its Raman peaks should be significantly different in energy position and number of nodes compared with Sb_2Se_3, which is the case for the peak around 250 cm^{-1}.

With the quality of the films investigated here, we cannot neglect other effects that may contribute to the observed Raman spectrum. In order to understand the RS peaks positions of Sb_2Se_3, we started to study the stability of the phase as function of incident RS laser power density. In other chalcopyrite materials, like for instance CIGS and CZTS, one needs to use relatively low values of laser power density in order to avoid damage to the film itself. The damage usually comes in 3 forms: i) structural changes that induce different symmetry space groups[25]; ii) evaporation of atoms of some elements which leads to a change in the structure[24]; and iii) incorporation and/or replacement of elements from the atmosphere, namely oxygen[24]. All of these changes have the potential to be thermodynamically available by the energy

delivered by the laser exposure. In this particular case, the amount of energy available to catalyze the possible changes comes from the laser power density and from relative long exposure times.

Having demonstrated further evidence that the Sb_2Se_3 phase should not have the 250 cm^{-1} peak, we will now explore its appearance. As previously referred, the appearance of new peaks, while changing the laser power density, can be a consequence of several causes. Since the FWHM values and the peak positions of the Sb_2Se_3 phase are kept the same as function of laser power density, we can discard structural changes since these would change the lattice parameters and/or change the space group leading to significant changes in the RS peaks. If the 250 cm^{-1} peak is to be associated with a Sb_2O_3 phase, then, oxygen can only come from two sources: i) oxygen already present on the sample surface due to air exposure after growth and/or b) oxygen present in the air.

To test the oxygen origin hypothesis, we performed a Raman laser power density dependence by inserting the sample in a microscope cryostat stage (Linkam 650) connected to a vacuum pump that allows to achieve a pressure of $\sim 5\times10^{-2}$ mbar. In this case, the samples might locally be heated to higher temperature values due to lack of convection and thus, there is a small chance that some peak position energy shifts might occur. FIG. 2a) shows, at low laser power density the same results as in the previous test are found: i) the Sb_2Se_3 can be identified with peaks at 153 cm^{-1}, 189 cm^{-1} and 210 cm^{-1}; ii) the trigonal Se phase is present with a double peak at 234 cm^{-1} and 239 cm^{-1}. With increasing laser power density, we see the same trend as observed previously: the double peak corresponding to trigonal Se lowers significantly while the Sb_2Se_3 peaks suffer very minor changes. At the highest laser power density values, a small peak around 250 cm^{-1} is present and no traces of the peak at 372 cm^{-1} are to be found. These results tend to indicate that under vacuum, the Se excess at the sample surface is removed, however, due to the lack of oxygen from the air, the formation of Sb_2O_3 is vastly reduced. The oxygen source can be attributed both to small amounts of oxygen adsorbed at the sample surface and to remaining oxygen still present in the low-vacuum conditions of the measurement.

The findings of the previous experiments allow us to conclude that, contrary to the literature, the peaks at 250 cm^{-1} and 372 cm^{-1} do not belong to Sb_2Se_3, but belong rather to Sb_2O_3. Furthermore, we hypothesize that the formation of the Sb_2O_3 is due to Se replacement by oxygen and resulting Se is simply evaporated due to its high vapor-pressure. The two-step reaction is represented by eq.1 and eq2:

$$Sb_2Se_3(s) + Se_2\,(s) \rightarrow Sb_2Se_3(s) + Se_2\,(g) \qquad \text{(eq. 1)}$$

$$2 \cdot Sb_2Se_3(s) + 3 \cdot O_2(g/s) \rightarrow 3 \cdot Sb_2O_3(s) + 3 \cdot Se_2\,(g) \qquad \text{(eq. 2)}$$

This system has not been studied in detail and no trusty values of enthalpy energies are available to evaluate the reactions likelihood. These reactions fit the observed results and thermodynamic studies are needed to validate them.

In order to validate even further our results, a detailed XRD temperature dependence study was carried from RT up to 500 °C. The temperature was increased in air atmosphere, performing effectively an in-situ air-annealing. In FIG. 2b) we present only the results obtained at RT and 450 °C, since above 450 °C the film sublimates due to the compound high values of vapor-pressure. At low temperature conditions, the x-ray diffractogram is dominated by the Sb_2Se_3 orthorhombic peaks[31]. At the temperature of 450 °C, the x-ray diffractogram starts to be dominated almost exclusively by the Sb_2O_3 diffraction peaks[31]. This result is further evidence that with enough energy, Sb_2Se_3 decomposes into Sb_2O_3. As in the Raman analysis, due to the significant difference in the crystalline structure between Sb_2Se_3 and Sb_2O_3, the diffraction pattern is significantly different as well.

Conclusions

In this work, we showed that the identification of Sb_2Se_3 using Raman scattering must be performed in low laser power density conditions, ~170 $MW.m^{-2}$, in order to avoid the Se evaporation and the oxidation of the Sb_2Se_3 phase. The prominent peak around 250 cm^{-1} which is usually attributed to Sb_2Se_3

in the literature, belongs in fact to Sb_2O_3. The origin of the Sb_2O_3 is due to oxidation. In order to avoid oxidation during RS measurements and to perform more reliable measurements, at high laser excitation power conditions it is recommended to perform this technique in vacuum or in an inert atmosphere environment. Alternatively, Raman Scattering measurements of Sb_2Se_3 should be done at very low laser power density conditions. We note that the observation of oxidation is true for a variety of measurements that are done in air and that provide some energy to the samples like XRD, photoluminescence, photoconductivity, etc. An important observation of our work is also related with the stability of the Sb_2Se_3 compound: high energy conditions, like excitation laser power or temperature, easily lead to the formation of a Sb_2O_3 phase, thus, synthesis processes have to account for this fact when preparing the compound.

Acknowledgements

P. M. P. Salomé acknowledges the funding of Fundação para Ciência e Tecnologia (FCT) through the project IF/00133/2015. B. Vermang has received funding from the European Research Council (ERC) under the European Union's Horizon 2020 research and innovation programme (grant agreement n° 715027). A. Shongalova acknowledges the funding of Erasmus + program 2016/17. This work was funded by FEDER funds through the COMPETE 2020 Programme and by FCT - Portuguese Foundation for Science and Technology under the projects UID/CTM/50025/2013.

REFERENCES

1. H. C. Kim, T. S. Oh, D.-B. Hyun. *Thermoelectric properties of the p-type Bi_2Te_3–Sb_2Te_3–Sb_2Se_3 alloys fabricated by mechanical alloying and hot pressing*. Journal of Physics and Chemistry of Solids **61,** 743–749 (2000).

2. M.-Z. Xue, Z.-W. Fu. *Pulsed laser deposited Sb_2Se_3 anode for lithium-ion batteries*. Journal of Alloys and Compounds **458,** 351–356 (2008).

3. J. Ma, Y. Wang, Y. Wang, Q. Chen, J. Lian, W. Zheng. *Controlled Synthesis of One-Dimensional Sb_2Se_3 Nanostructures and Their Electrochemical Properties*. The Journal of Physical Chemistry C **113,** 13588–13592 (2009).

4. W. Luo, A. Calas, C. Tang, F. Li, L. Zhou, L. Mai. *Ultralong Sb_2Se_3 Nanowire-Based Free-Standing Membrane Anode for Lithium/Sodium Ion Batteries*. ACS Applied Materials & Interfaces **8,** 35219–35226 (2016).

5. L. Wang, D.-B. Li, K. Li, C. Chen, H.-X. Deng, L. Gao, Y. Zhao, F. Jiang, L. Li, F. Huang, Y. He, H. Song, G. Niu, J. Tang. *Stable 6%-efficient Sb_2Se_3 solar cells with a ZnO buffer layer*. Nature Energy **2,** 17046 (2017).

6. Y. Zhou, L. Wang, S. Chen, S. Qin, X. Liu, J. Chen, D.-J. Xue, M. Luo, Y. Cao, Y. Cheng, E. H. Sargent, J. Tang. *Thin-film Sb_2Se_3 photovoltaics with oriented one-dimensional ribbons and benign grain boundaries*. Nature Photonics **9,** 409–415 (2015).

7. C. Chen, Y. Zhao, S. Lu, K. Li, Y. Li, B. Yang, W. Chen, L. Wang, D. Li, H. Deng, F. Yi, J. Tang. *Accelerated Optimization of TiO_2/Sb_2Se_3 Thin Film Solar Cells by High-Throughput Combinatorial Approach*. Advanced Energy Materials **7,** 1700866 (2017).

8. C. Chen, L. Wang, L. Gao, D. Nam, D. Li, K. Li, Y. Zhao, C. Ge, H. Cheong, H. Liu, H. Song, J. Tang. *6.5% Certified Efficiency Sb_2Se_3 Solar Cells Using PbS Colloidal Quantum Dot Film as Hole-Transporting Layer*. ACS Energy Letters **2,** 2125–2132 (2017).

9. X. Wen, Y. He, C. Chen, X. Liu, L. Wang, B. Yang, M. Leng, H. Song, K. Zeng, D. Li, K. Li, L. Gao, J. Tang. *Magnetron sputtered ZnO buffer layer for Sb_2Se_3 thin film solar cells*. Solar Energy Materials and Solar Cells **172,** 74–81 (2017).

10. A. P. Torane, C. H. Bhosale. *Preparation and characterization of electrodeposited Sb_2Se_3 thin films from non-aqueous media*. Journal of Physics and Chemistry of Solids **63,** 1849–1855 (2002).

11. X. Liu, J. Chen, M. Luo, M. Leng, Z. Xia, Y. Zhou, S. Qin, D.-J. Xue, L. Lv, H. Huang, D. Niu, J. Tang. *Thermal Evaporation and Characterization of Sb_2Se_3 Thin Film for Substrate Sb_2Se_3/CdS Solar Cells*. ACS Applied Materials & Interfaces **6,** 10687–10695 (2014).

12. M. Dimitrievska, G. Gurieva, H. Xie, A. Carrete, A. Cabot, E. Saucedo, A. Pérez-Rodríguez, S. Schorr, V. Izquierdo-Roca. *Raman scattering quantitative analysis of the anion chemical composition in kesterite $Cu_2ZnSn(S_xSe_{1-x})_4$ solid solutions*. Journal of Alloys and Compounds **628,** 464–470 (2015).

13. C. Insignares-Cuello, F. Oliva, M. Neuschitzer, X. Fontané, C. Broussillou, T. Goislard de Monsabert, E. Saucedo, C. M. Ruiz, A. Pérez-Rodríguez, V. Izquierdo-Roca. *Advanced characterization of electrodeposition-based high efficiency solar cells: Non-destructive Raman scattering quantitative assessment of the anion chemical composition in $Cu(In,Ga)(S,Se)_2$ absorbers*. Solar Energy Materials and Solar Cells **143,** 212–217 (2015).

14. P. Salomé, P. Fernandes, J. Leitão, M. Sousa, J. P. Teixeira, A. F. da Cunha. *Secondary crystalline phases identification in $Cu_2ZnSnSe_4$ thin films: Contributions from Raman scattering and photoluminescence*. Journal of Materials Science **49,** 7425–7436 (2014).

15. Y. Zhang, G. Li, B. Zhang, L. Zhang. *Synthesis and characterization of hollow Sb_2Se_3 nanospheres*. Materials Letters **58,** 2279–2282 (2004).

16. Y. Zhou, M. Leng, Z. Xia, J. Zhong, H. Song, X. Liu, B. Yang, J. Zhang, J. Chen, K. Zhou, J. Han, Y. Cheng, J. Tang. *Solution-Processed Antimony Selenide Heterojunction Solar Cells*. Advanced Energy Materials **4,** 1301846 (2014).

17. K. Nagata, K. Ishibashi, Y. Miyamoto. *Raman and Infrared Spectra of Rhombohedral Selenium*. Japanese Journal of Applied Physics **20,** 463–469 (1981).

18. G. Mestl, P. Ruiz, B. Delmon, H. Knozinger. *Sb_2O_3/Sb_2O_4 in reducing/oxidizing environments: an in situ Raman spectroscopy study*. The Journal of Physical Chemistry **98,** 11276–11282 (1994).

19. Y. Zhao, K. T. E. Chua, C. K. Gan, J. Zhang, B. Peng, Z. Peng, Q. Xiong. *Phonons in Bi_2S_3 nanostructures: Raman scattering and first-principles studies*. Phys. Rev. B **84,** 205330 (2011).

20. V. S. Minaev, S. P. Timoshenkov, V. V Kalugin. *Structural and phase transformations in condensed selenium*. Journal of Optoelectronics and Advanced Materials **7,** 1717–1741 (2005).

21. C. Platzer-Björkman, P. Zabierowski, J. Pettersson, T. Törndahl, M. Edoff. *Improved fill factor and open circuit voltage by crystalline selenium at the Cu(In,Ga)Se_2 /buffer layer interface in thin film solar cells*. Progress in Photovoltaics: Research and Applications **18,** 249–256 (2010).

22. A. SeJin, K. Ki Hyun, Y. Jae Ho, Y. Kyung Hoon. *Effects of selenization conditions on densification of Cu(In,Ga)Se_2 (CIGS) thin films prepared by spray deposition of CIGS nanoparticles*. Journal of Applied Physics **105,** 113533 (2009).

23. Z. Li, X. Chen, H. Zhu, J. Chen, Y. Guo, C. Zhang, W. Zhang, X. Niu, Y. Mai. *Sb_2Se_3 thin film solar cells in substrate configuration and the back contact selenization*. Solar Energy Materials and Solar Cells **161,** 190–196 (2017).

24. *Raman Scattering in Materials Science*. **42,** (Springer Berlin Heidelberg, 2000).

25. D. Bäuerle. *Laser Processing and Chemistry*. (Springer Berlin Heidelberg, 2011). doi:10.1007/978-3-642-17613-5

26. P. Sereni, M. Musso, P. Knoll, P. Blaha, K. Schwarz, G. Schmidt. *Polarization-Dependent Raman Characterization of Stibnite (Sb_2S_3)*. in *AIP Conference Proceedings* **1267,** 1131–1132 (2010).

27. R. Caracas, X. Gonze. *First-principles study of the electronic properties of A_2B_3 minerals, with A=Bi,Sb and B=S,Se*. Physics and Chemistry of Minerals **32,** 295–300 (2005).

28. J. Wang, Z. Deng, Y. Li. *Synthesis and characterization of Sb_2Se_3 nanorods*. Materials Research Bulletin **37,** 495–502 (2002).

29. Z. G. Ivanova, E. Cernoskova, V. S. Vassilev, S. V Boycheva. *Thermomechanical and structural characterization of $GeSe_2$–Sb_2Se_3–ZnSe glasses*. Materials Letters **57,** 1025–1028 (2003).

30. I. Efthimiopoulos, J. Zhang, M. Kucway, C. Park, R. C. Ewing, Y. Wang. *Sb_2Se_3 under pressure*. Scientific Reports **3,** 2665 (2013).

31. *International Centre for Diffraction Data—Reference Code, 01-072-1184 (Orthorhombic Pbnm Sb_2Se_3), 01-072-1334 (cubic Fd-3m Sb_2O_3), 00-005-0562 (Rhombohedral R-3m Se_6)*.

32. X. Wang, K. Kunc, I. Loa, U. Schwarz, K. Syassen. *Effect of pressure on the Raman modes of antimony*. Physical Review B **74,** 134305 (2006).

Table 1- Main RS peaks of several phases that may originate during the growth of Sb_2Se_3. As explained further in the text, the orthorhombic Sb_2Se_3 is intentionally without a peak at 250 cm^{-1} and this region is highlighted in the other phases.

Compound	**Structure**	**Raman shift (cm^{-1})**	**Supporting references**
Sb_2Se_3	orthorhombic	80,120,151, 189, 210	this work, [29]
Sb_2O_3	cubic	82, 189, 254, 373,450	[18], this work
Sb_2O_4		72, 142, 199, 255, 400, 463	[18]
Se_n (spiral chains)	trigonal	141, 234, 237	[14,17,20], this work
Se_8 (rings)	α-monoclinic	112, 253	[17,20]
Se_6 (rings)	rhombohedral	67-72, 102, 129, 221, 247	[17]
Red Se (rings)	amorphous	250	[14,17,20]
Sb	rhombohedral	110, 150	[32]

List of figure

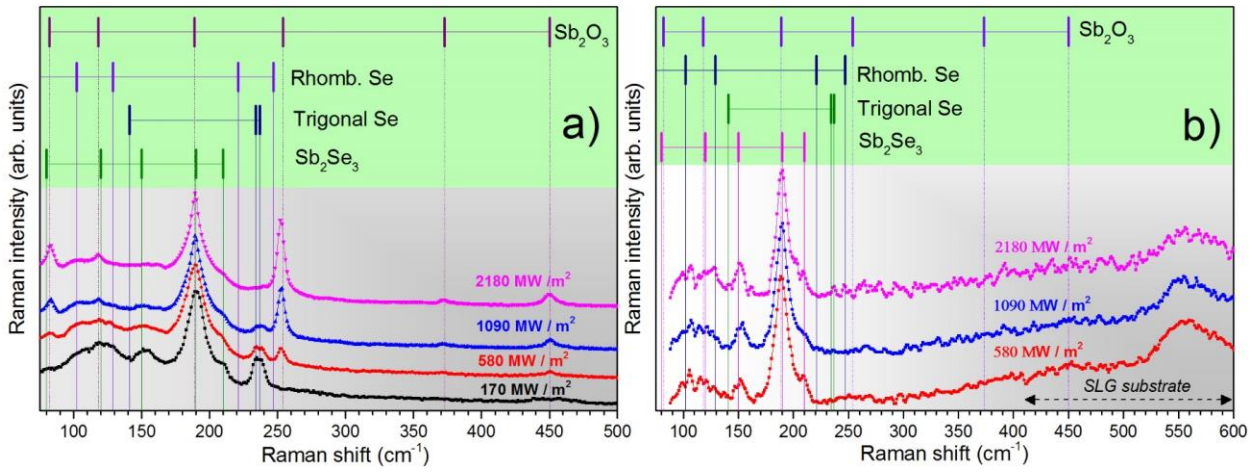

Fig1

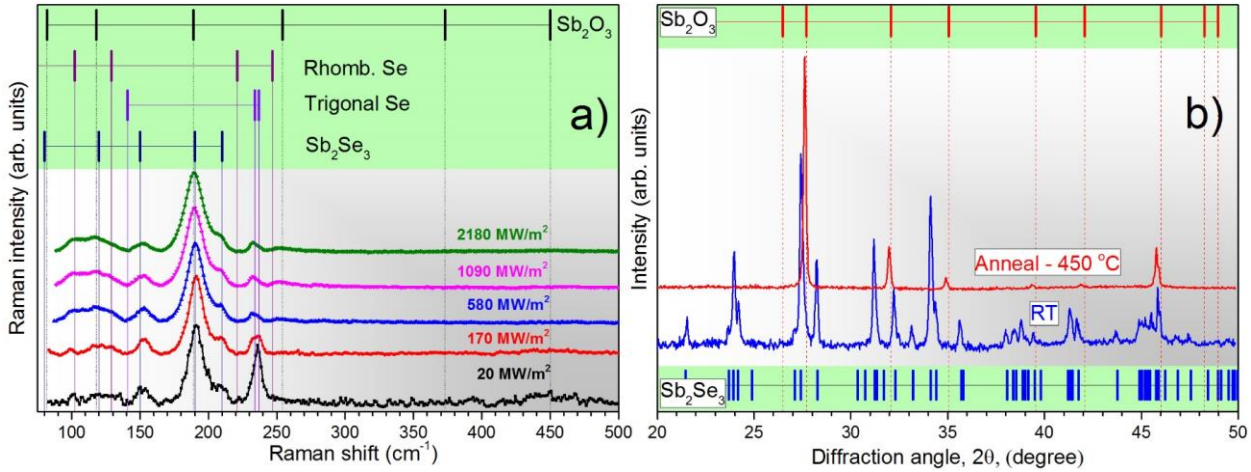

Fig2

List of figure captions

FIG. 1 a) Study of Raman spectrum dependence on the laser power density excitation for a Sb_2Se_3 film at room temperature. Under the lowest laser power density, the peak at 250 cm^{-1} is absent in spite of several Sb_2Se_3 peaks being present. b) Raman spectrum dependence on the excitation laser power density measured for the cross section of the analyzed film, in a spot close to the sodium lime glass substrate (SLG). The Raman mode assignment for Sb_2O_3, Rhomb. Se, Trigonal Se and Sb_2Se_3 were done according references in table 1.

FIG. 2 a) Raman laser power density dependency test in low-vacuum conditions. With increasing power density, it is observable a lowering of the peak associated with selenium and only a very small and broad peak at 250 cm^{-1} is found at high power conditions. The peaks attributed to the phase Sb_2Se_3, 153 cm^{-1}, 189 cm^{-1} and 210 cm^{-1}, remain unchanged. The Raman mode assignment for Sb_2O_3 Rhomb. Se, Trigonal Se and Sb_2Se_3 were done according references in table 1. b) Diffractogram of the Sb_2Se_3 thin film at room temperature and at a temperature of 450 °C. The indexation of Sb_2Se_3 XRD peaks[31] is also included.